Monte Carlo Simulations of Water Exchange Through Myelin Wraps: Implications for Diffusion MRI

Lorenza Brusini, Gloria Menegaz, and Markus Nilsson

***Abstract*— Diffusion magnetic resonance imaging (dMRI) yields parameters sensitive to brain tissue microstructure. A structurally important aspect of this microstructure is the myelin wrapping around the axons. This paper investigated the forward problem concerning whether water exchange via the spiraling structure of the myelin can meaningfully contribute to the signal in dMRI. Monte Carlo simulations were performed in a system with intra-axonal, myelin, and extra-axonal compartments. Diffusion in the myelin was simulated as a spiral wrapping the axon, with a custom number of wraps. Exchange (or intra-axonal residence) times were analyzed for various number of wraps and axon diameters. Pulsed gradient sequences were employed to simulate the dMRI signal, which was analyzed using different methods. Diffusional kurtosis imaging analysis yielded the radial diffusivity (RD) and radial kurtosis (RK), while the two-compartment Kärger model yielded estimates the intra-axonal volume fraction (v_{ic}) and exchange time (τ). Results showed that τ was on the sub-second level for geometries with axon diameters below 1.0 μm and less than eight wraps. Otherwise, exchange was negligible compared to typical experimental durations, with τ of seconds or longer. In situations where exchange influenced the signal, estimates of RK and v_{ic} increased with the number of wraps, while RD decreased. τ estimates from simulated signals were in agreement with predicted ones. In conclusion, exchange through spiraling myelin permits sub-second τ for small diameters and low number of wraps. Such conditions may arise in the developing brain or in neurodegenerative disease, and thus the results could aid the interpretation of dMRI studies.**

***Index Terms*— PGSTE, exchange time, kurtosis, T_2 relaxation, Kärger.**

Manuscript received September 13, 2018; revised December 1, 2018; accepted January 13, 2019. Date of publication February 27, 2019; date of current version May 31, 2019. This work was supported in part by the Swedish Research Council under Grant 2016-03443, in part by the Swedish Foundation for Strategic Research under Grant AM13-0090, and in part by the CR Award under Grant MN15. *(Corresponding author: Lorenza Brusini.)*

L. Brusini and G. Menegaz are with the Department of Computer Science, University of Verona, 37134 Verona, Italy (e-mail: lorenza.brusini@univr.it).

M. Nilsson is with the Department of Clinical Sciences Lund, Diagnostic Radiology, Lund University, 22100 Lund, Sweden.

This paper has supplementary downloadable material available at http://ieeexplore.ieee.org, provided by the author.

Color versions of one or more of the figures in this paper are available online at http://ieeexplore.ieee.org.

Digital Object Identifier 10.1109/TMI.2019.2894398

I. Introduction

DIFFUSION Magnetic Resonance Imaging (dMRI) has increased our understanding of the relationship between the microstructure of white matter and the brain connectivity [1]. Custom image acquisitions may yield functional information on the white matter microstructure, for example, axon diameters [2], microscopic anisotropy [3]–[5], and membrane permeability or water exchange rates [6]–[10]. In the context of exchange, it is unknown how the structure of the myelin affects the dMRI signal. Gaining such knowledge is important for the interpretation of dMRI results in maturation, aging, and neurological disorders.

Myelin is a membranous structure that wraps axons with multiple lipid bilayers [11], [12], which limits the rate of water exchange between the intra- and extra-axonal spaces. Water nevertheless is present in the spaces between the bilayers, and can be identified by its short transverse relaxation time (T_2) [13]. Due to the short T_2, many models used to analyze dMRI data include the assumption that the myelin does not contribute to the observed signal. However, some approaches include water exchange between the intra- and extra-axonal space. These have resulted in a wide range of estimated exchange times. Nilsson *et al.* [9] found exchange times in healthy white matter in order of seconds ($1.25-2.5$ s) whereas Nedjati-Gilani *et al.* [14] found values in the subsecond range ($0.5-0.6$ s).

To better understand the relation between white matter microstructure and expected exchange times in dMRI, simulations of water diffusion can be used. Most prior studies have, however, simulated axons as parallel semi-permeable cylinders, with exchange implemented as a direct jump from the intra to extra-axonal space, without considering the myelin [6], [7], [14], [15]. A few studies included more complex simulations. Nilsson *et al.* [8] investigated water exchange at the gaps occurring along a myelinated axon where the axolemma is exposed to the extracellular space (nodes of Ranvier). Hwang *et al.* [16] developed a histology-based diffusion simulation method with different diffusivities in each compartment, including the myelin sheath. Sen and Basser [17] proposed a model for diffusion in white matter as an array of identical thick-walled cylindrical tubes periodically arranged in a regular lattice and inserted in an

outer medium. Peled [18] studied a tensor model with an added baseline correlating with intra-axonal water volume on a geometry composed by coated parallel identical cylinders in a hexagonal lattice where particles were allowed to diffuse inside and through compartments. Baxter and Frank [19] added different spin concentrations for each compartment to the analysis described by Sen and Basser. To the best of our knowledge, [20] is the only study to pay attention to the multi-wrapping nature of the myelin, albeit implicitly, by modeling diffusion in myelin as anisotropic with a higher diffusivity in the tangential compared to radial direction [20].

This work explores which axonal geometries permit fast exchange, defined as sub-second exchange times. The geometry is so complex that simplifying assumptions are required to approach the problem. Molecules may move through the myelin spiral, exchange at the nodes of Ranvier or jump across each of the bilipid membranes that make up the myelin sheath, with different rates. Here, we chose to investigate the first of these three potential exchange mechanisms. Monte Carlo (MC) simulations were performed where the myelin was modeled as a spiral along which the water molecules could diffuse freely thanks to a different step generation mechanism. This configuration would reproduce the histologically known structure of myelin. The dependence of the exchange time (τ) on the myelin structure was investigated by varying the geometrical parameters. The myelin bilayers were considered to be impermeable, in order to study the through-spiral exchange mechanism in isolation. Effects of T_2 relaxation were also investigated. Diffusion-weighted signals from a pulsed gradient sequence were then simulated with experimental parameters suitable for clinical MRI. The simulated signal data was subsequently analyzed with the diffusional kurtosis imaging (DKI) model [21] and the modified Kärger model [22]. DKI was used to probe the response on summative variables such as the radial diffusivity (RD) and radial kurtosis (RK). The Kärger model was used to specifically analyze whether exchange times estimated from simulated signal data agreed with independent results from particle simulations.

II. Methods

Microstructure information is in dMRI encoded as a signal attenuation, due to a phase dispersion caused by the interaction of magnetic field gradients and diffusing spins. In the MC approximation, spins are represented by particles having a phase ϕ, which shapes the signal according to

$$S = \frac{1}{n}\sum_{k=1}^{n} w_k \exp(-i\phi_k), \tag{1}$$

where n is the number of particles, w_k a relaxation-weighting factor, $i^2 = -1$, and

$$\phi_k = \gamma \sum_{j=1}^{m} g_j\, x_j\, \Delta t \tag{2}$$

where γ is the gyromagnetic ratio, g_j the magnetic-field gradient discretized into m time points, x_j the position of the particle at time $t = j\Delta t$, and Δt is the time discretization of the simulation. The gradient waveform consisted of a pair of pulsed gradients, which can be described by two timing parameters: δ, which is the duration of each gradient pulse, and Δ which corresponds to the time between the firsts edges of the pulses. Imaging gradients were not considered.

Note that the diffusion time is given by $T_D = \Delta - \delta/3$ and the b-value by $b = \gamma^2\delta^2G^2T_D$, where G is the gradient amplitude of the pulsed gradients.

Effects of transverse relaxation were included via the weighting term w_k, which was computed according to

$$w_k = \prod_{c=1}^{3} \exp(-t_{c,k}/T_{2;c}) \tag{3}$$

where $T_{2;c}$ is the T_2-relaxation time for compartment c, and $t_{c,k}$ was obtained by tracking the time each particle spent in each compartment. Since a stimulated echo sequence was simulated, the only time points that contributed towards the $t_{c,k}$ were those when the simulated spins were in transversal mode. Longitudinal relaxation (T_1) was not included because it is considerably slower than the transverse relaxation.

A. Simulation Setup

The simulation geometry comprised three compartments: intra-axon, extra-axon and myelin, as illustrated in Fig. 1. Periodic boundary conditions were simulated through an infinite number of two-dimensional transversal sections ("units") of parallel cylinders representing axons. Each square unit comprised extra-axonal space around the axon and myelin, which were placed in the center of the unit. The width of the unit cell in the regular packing (s_{width}) was an adjustable parameter, together with the axon inner diameter (d_{inner}) and the g-ratio. The g-ratio was calculated as $g = d_{\text{inner}}/D_{\text{outer}}$, where D_{outer} was the outer diameter of the myelin. Another parameter was the number of myelin wraps (n_{wraps}) around the axon given the thickness.

In summary, the variables of the simulation model were: s_{width}, d_{inner}, g-ratio and n_{wraps}. Throughout this work, the g-ratio was set to $g = 0.7$ and s_{width} was derived from setting $\nu_{ic} = 0.45$, while d_{inner} and n_{wraps} were varied. Fig. 1A shows an example of the geometry with varying d_{inner} and n_{wraps} while maintaining g-ratio and s_{width} constant. Fig. 1B illustrates the periodic boundary conditions.

Myelin was implemented as a one-dimensional spiraling compartment. This choice was made due to the large difference in size between axon and myelin: the extracellular space between the myelin wraps is approximately 3.0 nm thick [12] whereas the axon diameter is generally between 0.4 and 4.0 μm in the brain [23]. Fig. 1C illustrates the geometrical equivalence of the described substrate model, as the intra-axonal space separated from the extra-axonal space by a long but thin wire. The intrinsic diffusivity was kept constant in all three compartments, which was ensured by keeping the step size constant.

A random walk on a discrete lattice was implemented by allowing particles to move inside axonal or extra-axonal space along a random direction in the xy-plane at each unit of time, with a step length of Δx. Particles were not allowed

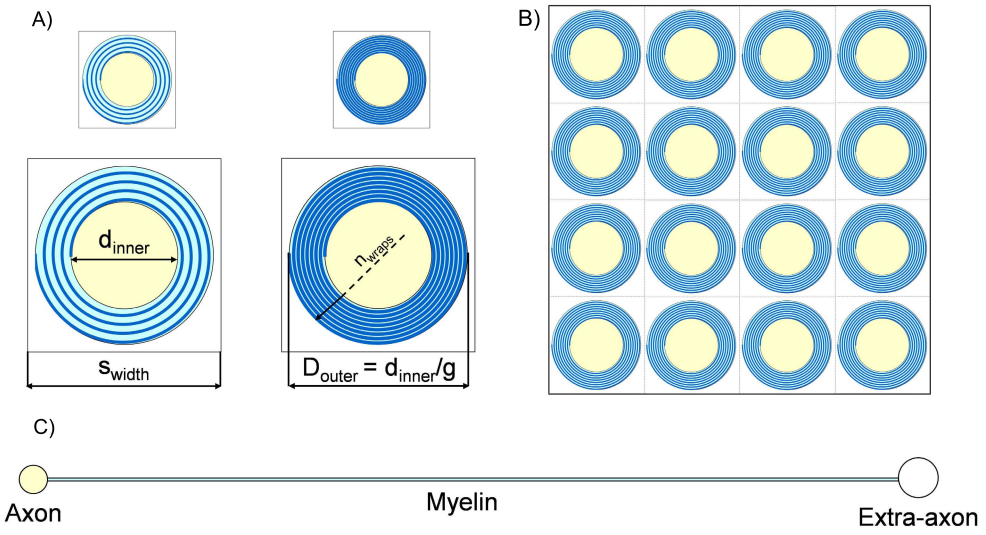

Fig. 1. Simulation setup. A) Changes of the axon diameter and number of wraps are illustrated across rows and columns, respectively. B) Periodic boundary conditions. C) Rectified myelin wraps as in the implementation.

to change compartments, except under specific conditions described in the next section. Inside the myelin spiral, positions were parameterized by an angle θ, computed as

$$\theta_k = l_k \Delta x / L n_{\text{wraps}} 2\pi \tag{4}$$

where l_k is the position along the spiral. Particles in the myelin took a random positive or negative unit step along l_k for each unit of time. Angles were transformed to positions according to

$$x = \left(\frac{d_{\text{inner}}}{2} + s\theta\right)\cos(\theta) \tag{5}$$

$$y = \left(\frac{d_{\text{inner}}}{2} + s\theta\right)\sin(\theta) \tag{6}$$

where s was the spacing between each arm [$s = (D_{\text{outer}} - d_{\text{inner}})/(4\pi n_{\text{wraps}})$]. The length of the spiral was calculated by solving

$$L = \int_0^{2\pi n_{\text{wraps}}} \sqrt{s^2 + \left(\frac{d_{\text{inner}}}{2} + s\theta\right)^2}\, d\theta. \tag{7}$$

Exchange was implemented by allowing the transition from axon to myelin (p_{am}), from myelin to axon (p_{ma}), from extra-axon to myelin (p_{em}) and from myelin to extra-axon (p_{me}) at specific points in the axonal and extra-axonal space (Fig. 2) while particles that hit the myelin in other points undergo to a re-generation of the random jump. These probabilities were constrained by equilibrium conditions of mass balance according to:

$$M_m \cdot p_{ma} = M_a \cdot p_{am} \tag{8}$$

$$M_m \cdot p_{me} = M_e \cdot p_{em} \tag{9}$$

where M_m, M_a and M_e are the total number of particles ("masses") in the myelin, axon and extra-axonal space, respectively. Since the myelin space was represented differently from the axon and extracellular spaces, the initial particle concentrations in each space was computed by counting pixels occupied by each compartment multiplied by the respective

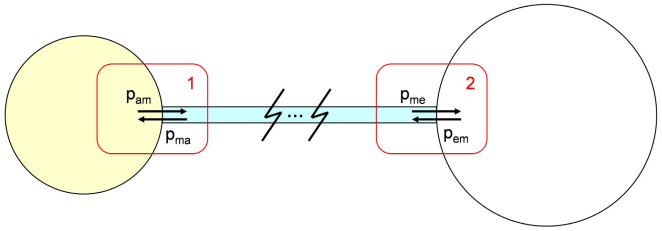

Fig. 2. Exchange setup. Referring to the geometrical equivalence of the cell unit for the implementation, the impermeability of the myelin walls is shown except for the myelin-to-axon and the myelin-to-extra areas highlighted by areas 1 and 2 respectively. In these areas, particles flow is allowed in both the directions.

spin concentration. For myelin, the concentration depended on the ratio between the probability to enter and leave it. These were computed as follows:

$$\begin{aligned} p_{ma} &= 1.0 \\ p_{am} &= p_{ma} \cdot \frac{A_m}{A_a} \\ p_{me} &= 1.0 \\ p_{em} &= p_{me} \cdot \frac{A_m}{A_e}. \end{aligned} \tag{10}$$

We assumed no hindrance for particles entering the myelin, except that the "cross sectional area" of the myelin layer was smaller than the simulated voxels. Thus, the axon-to-myelin transition area (A_m) was set to the width of the myelin water layer (3.0 nm [12]) whereas the myelin-to-axon and myelin-to-extra areas (A_a and A_e, respectively) were set to Δx.

B. Simulations

In the subsequent two-dimensional simulations, the number of particles used was $n = 100000$, diffusivity $D = 2.0\ \mu\text{m}^2/\text{ms}$, $\Delta x = 0.05\ \mu\text{m}$ and 100 equally spaced b-values were chosen from 0 to 2500 s/mm^2.

1) Simulation Set #1: Observable τ: The first set of simulated experiments were designed to probe how the intra-axonal

residence time, referred to as the exchange time, depends on myelin properties. Particles were thus initialized in the intra-axonal and myelin spaces only. Exchange into the extra-axonal space was allowed, but particles were not allowed to re-enter the myelin. This setup gives an unbiased measure of τ [7]. Random walks were then simulated for a period of 200 ms and the number of intra-axonal particles as a function of time was recorded. τ was computed from the following relation,

$$n(t) = n(0)\exp(-t/\tau), \tag{11}$$

via polynomial fitting of $\log n(t)$ in a least-squares sense. The least-squares fit was performed on the linear relation of the log of the particles concentration per unit of time. In particular, the polyfit command in Matlab was employed and used to extract τ calculating the negative reciprocal of the fitting result.

Effects on the exchange times were investigated in two fundamental cases. First we investigated effects of the number of myelin turns (τ versus n_{wraps}), and then of the axon diameter (τ versus d_{inner}). In the first case, d_{inner} was varied between 1.0 and 2.0 μm and n_{wraps} between 1, 2, 4, 8, 16 and 32. In the second case n_{wraps} was varied between 1 and 4 and d_{inner} between 1.0, 2.0 and 4.0 μm. For reference, please note that the median axon diameter in the planum temporale sector of the human corpus callosum was recently reported to be 0.89 μm [24].

2) Simulation Set #2: PGSTE Simulation: Pulsed-gradient stimulated echo (PGSTE) acquisitions were simulated with a diffusion encoding time of $\delta = 15$ ms, and three different Δ of 25, 55 and 225 ms. The mixing time corresponded to Δ (25, 55 and 255 ms, respectively) while the echo time was limited to time of the two gradient pulses 2δ (30 ms).

3) Simulation Set #3: RD and RK Estimates: The DKI model [21] was fitted to the PGSTE simulated signal for $\delta = 15$ ms and $\Delta = 25$ ms for two different choices of myelin T_2 relaxation: short ($T_2 = 15$ ms) and long ($T_2 = 85$ ms), while the T_2 was set to 85 ms for both the axon and extra-axon compartments [20].

Following the one-dimensional perpendicular acquisition scheme, the model was formalized as follows:

$$S(b) = S_0 \cdot \exp\left[-b \cdot RD + (b \cdot RD)^2 RK/6\right]. \tag{12}$$

The free parameters of the model S_0, RD and RK were obtained through nonlinear curve-fitting in least-squares sense via the Levenberg-Marquardt algorithm without enforcing a negative first derivative. The initial parameter guesses that we chose were the simulated S_0, $\sim$0 m^2/ms for RD and $\sim$0 for RK.

In addition, the apparent fiber density (AFD) was calculated as the diffusion signal value at the highest b-value (2500 s/mm^2). This measure calculated in radial direction with respect to the substrate provides an estimation of v_{ic} [25].

4) Simulation Set #4: τ Value Estimate: The PGSTE synthetic signals were used to fit the Kärger model [22]. More in detail, the two-compartment model was the same as in [7]:

$$S(b) = S_0\begin{bmatrix}1 & 1\end{bmatrix}\exp(-b \cdot \mathbf{ADC} + \mathbf{K} \cdot T_D)\begin{bmatrix}v_{ic}\\ v_{ec}\end{bmatrix} \tag{13}$$

where $v_{ec} = 1 - v_{ic}$; **ADC** was defined as follows:

$$\mathbf{ADC} = \begin{bmatrix}ADC_{ic} & 0\\ 0 & ADC_{ec}\end{bmatrix} \tag{14}$$

with ADC_{ic} calculated as in [7]; and **K** was formalized as:

$$\mathbf{K} = \begin{bmatrix}-k_{ec} & k_{ic}\\ k_{ec} & -k_{ic}\end{bmatrix} \tag{15}$$

where k_{ec} and k_{ic} were the exchange rates in respectively intra- and extracellular compartments related by $k_{ec}v_{ec} = k_{ic}v_{ic}$ and $k_{ic} = 1/\tau$.

The free parameters S_0, ADC_{ec}, τ and v_{ic} were recovered by nonlinear curve-fitting in least-squares sense via the trust-region-reflective algorithm. The diameter was fixed in a negligible range given that the axons' diameter was below the resolution limit of dMRI [26].

Moreover, 500 instances of Gaussian noise (signal to noise ratio $SNR = 40$) were added to each considered diffusion signal and the 5^{th} and 95^{th} percentiles of the estimated parameters distributions were calculated.

III. Results

A. MC Simulator Validation

The MC simulator was validated by experiments comparing the results with well known ground truths. Results are reported in Supplementary Materials.[1] In particular, simulations of free and restricted diffusion were found to agree with theoretical predictions. The transition between compartments was also tested by studying the concentration trends in each compartment during 200 ms. The test was performed for transition probabilities both allowed and not, and the negligible slope of the number of particles versus time in both cases confirmed that the initial system was in equilibrium and that the exchange mechanism was correctly implemented. The time tracking of the particles was checked by using the same simulation set of the restricted diffusion validation test with particles distributed in all compartments. Since no transition was allowed, the equality between the time spent in each compartment and the total time required for the acquisition sequence proved the correctness of the simulation. The T_2 relaxation was assessed using the same simulation set of the free and restricted diffusion validations. The results were validated by comparing the signals to the theoretical ones modulated by the term $\exp(-T_{\text{tot}}/T_2)$.

B. Simulations

1) Simulation Set #1: Fig. 3A shows observable τ values as a function of n_{wraps} for two different d_{inner}. In particular, water particles escaped slower from axons adding wraps, and τ values were systematically higher for larger d_{inner}. Fig. 3A shows the axon water concentration versus time decaying trend, from which τ could be recovered.

Fig. 3B illustrates how exchange times depend on d_{inner}. Exchange times were longer for larger axons and in axons with more myelin wraps. In both cases, y-axis was limited

[1]Supplementary materials are available in the supporting documents/multimedia tab.

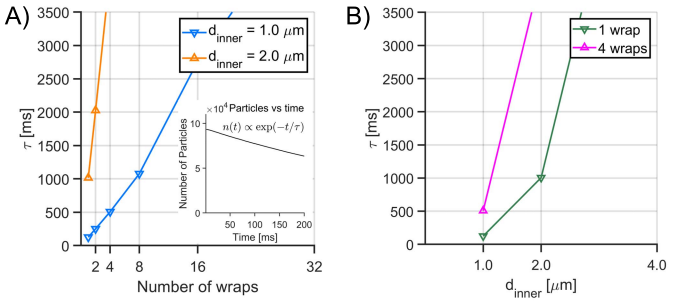

Fig. 3. Exchange time observed as the time taken by water particles for escaping from axon into extra-axon depending on A) the number of wraps for axon diameter 1.0 and 2.0 μm, B) the axon diameter for 1 and 4 myelin wraps. In A) is also reported the axon water particles versus time curve for axon diameter 1.0 μm and 4 wraps.

to 3500 ms to highlight only configurations where τ can be expected to be recoverable with current MRI acquisitions [9].

2) Simulation Set #2: The simulated diffusion signals curves are illustrated in Fig. 4, which shows that less myelin wraps resulted in stronger signal attenuation. The signal generated in the geometry with the highest number of wraps did not change with varying T_D, while in the ones with smaller n_{wraps} the attenuation increased with T_D. Moreover, differences in Fig. 4A and 4B highlighted a larger sensitivity to n_{wraps} variations when d_{inner} was small.

3) Simulation Set #3: Model parameters from DKI are shown in Fig. 5A and 5B. Fig. 5C shows the signal at the highest b-value, which is referred to as AFD. The values of RD generally decreased with increasing n_{wraps} in the range $0.62-0.46$ μm^2/ms, while RK and AFD increased. Values of RK varied in the range $1.75-2.67$ while AFD varied between 0.42 and 0.56. A larger slope of RD, RK and AFD versus n_{wraps} curves were observed for longer myelin T_2 relaxation. Moreover, for long myelin T_2 relaxation the curve representing small axons overcame the bigger axon curve at lower n_{wraps} (16 wraps) compared to short myelin T_2 relaxation for all parameters.

4) Simulation Set #4: Fig. 6 shows the parameters estimated via Kärger model fitting. The estimated v_{ic} slightly increased with n_{wraps}, and almost negligible error areas were identified ranging from 0.41 to 0.52. No large differences were observed in v_{ic} when changing d_{inner}. The ADC_{ec} estimate was not highly sensitive to n_{wraps} or d_{inner}, and errors were negligible. Estimated values of τ behaved as ground truth values in Fig. 3A, showing higher values for larger d_{inner} and higher values of n_{wraps}. However, Fig. 6C shows larger estimation uncertainty at larger values of n_{wraps}. Numerical details are provided in Table I, highlighting a good agreement between ground-truth observable exchange times and the exchange times estimated by the model fit for sub-second exchange times, but large uncertainties otherwise.

IV. Discussion

This work targeted the impact of the spiraling myelin structure for explaining water exchange in white matter. To the best of our knowledge, this was the first time that the spiraling nature of myelin was directly mimicked in simulations. Other studies have simulated the myelin structure indirectly, for example, by a compartment with different diffusivity in the radial and circumferential directions [20]. Understanding the impact of myelin on exchange is important as it would contribute to determine the value of τ in white matter for which an agreement is still missing in [9], [14], and [27]–[29].

We found that small axons with few myelin wraps could yield sub-second exchange times. Such short exchange times were within the same order of magnitude as those retrieved in rat brains [28], [29]. Note that axons in the rat brain are potentially smaller and have fewer myelin wraps compared to human axons [11]. Exchange times longer than a second were found for diameters of above approximately 2.0 μm and in presence of more than approximately 8 myelin wraps. These findings were in line with what observed by Dula *et al.* [30] and Harkins *et al.* [31] according to which exchange is slower in large axons and in axons with thick myelin. In the human brain, most axons have diameters below 2.0 μm [23], [24], but for most axons in healthy white matter we expect more than approximately 10 myelin wraps or more [11], [32]. Our results thus support the assumption of slow (negligible) exchange in healthy white matter. This result is more in line with the findings of Nilsson and colleagues [9] than with those of Nedjati-Gilani and colleagues [14]. During development or degeneration, the myelin structure can change and the number of wraps can shrink [32]–[34], which may reduce the exchange times. In such cases, measurement of exchange times could become clinically feasible.

From a mechanistic point of view, we found that the observable exchange times increased with the number of wraps and for larger axons. This is intuitively understandable since the length of the path the spins have to travel to exit the axon through the myelin sheet increases with n_{wraps}, and thus the time spent in the spiral. τ was also greater in larger axons. From our results, we can extrapolate some scaling laws. Knowing that the surface-to-volume ratio in a cylinder is determined by the radius (r) as $A/V = 4/r$, we know that $\tau \propto r/K$, where K represents an equal permeability along the whole membrane area. In the case of a cylinder covered by a spiraling impermeable membrane, however, the permeability is high only where the spiral opens towards the cylinder, and zero elsewhere. The factor governing the exchange rate will then be the width of the space between the turns of the spiral. We thus get $\tau \propto r^2/K_m A_m$, where A_m is the area of the spiral opening. This law would explain the scaling with r^2 in Fig. 3. Another aspect that could be of interest to explore but is out of the scope of this study is the modulation of the ADC_{ec} which, in contrast to exchange [35], is a first-order effect (b or q^2) and for which the outer radius and the surface-to-volume ratio would be a reasonable parametrisation.

From the perspective of the signal-versus-b curves, we found a larger attenuation in simulated axons with smaller n_{wraps}. This effect was accentuated with longer diffusion times, in line with [6] and [36]. This result is also in agreement with the findings of Harkins and Does [20], who found that slower diffusion in the myelin (in this study given by many n_{wraps}) accounted for more signal coming from water staying in the multi-wrapping compartment.

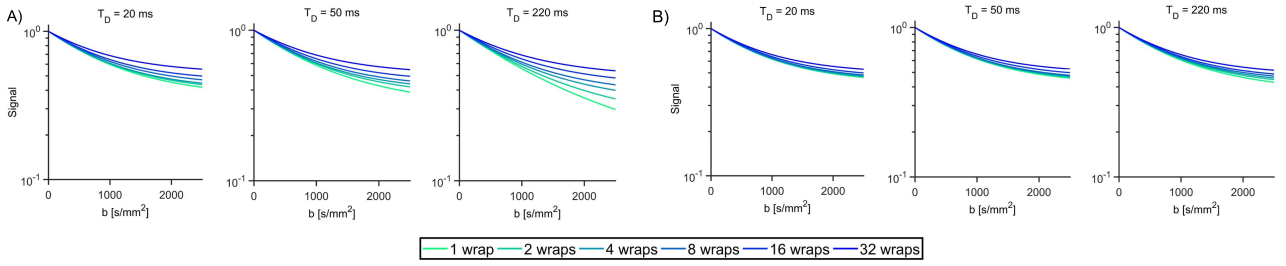

Fig. 4. PGSTE simulated diffusion signal varying the number of myelin wraps (*light blue - blue colors*) and diffusion time (*columns*) for axons having diameter A) 1.0 μm and B) 2.0 μm.

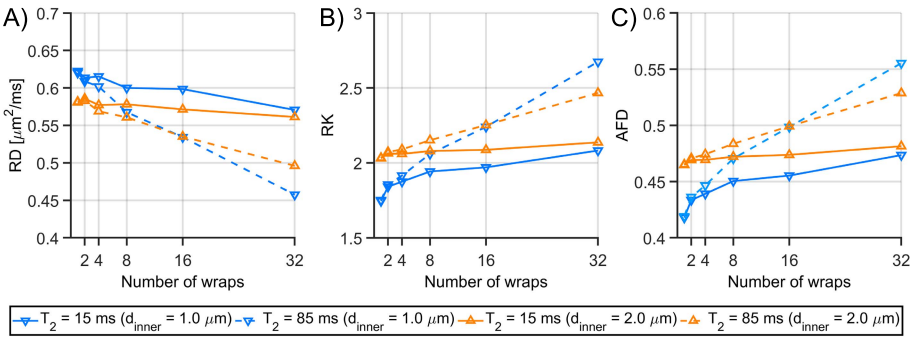

Fig. 5. DKI model estimated parameters in case of axon diameter 1.0 and 2.0 μm and short (*solid line*) and long (*dashed line*) myelin T_2 relaxation: A) radial diffusivity, B) radial kurtosis and C) apparent fiber density.

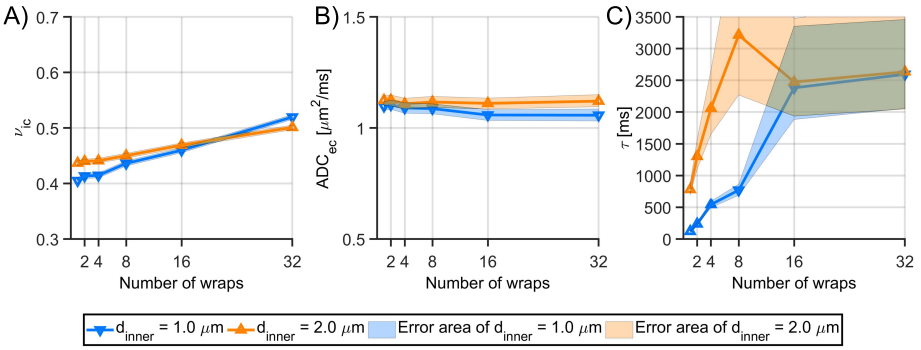

Fig. 6. Kärger model estimated parameters in case of axon diameter 1.0 and 2.0 μm: A) intracelullar volume fraction, B) extracellular apparent diffusion coefficient and C) exchange time. Error areas are limited by 5^{th} and 95^{th} percentiles computed on 500 noisy instances of signal ($SNR = 40$).

After fitting the DKI model, we could observe that RD decreases and RK increases with the number of wraps. The ranges of these values were similar to those found by Harkins and Does [20]. As for the AFD, we expected it to be proportional to v_{ic} [25], but found that it increased with n_{wraps}. This finding was in line with what found by Peled [18], who showed that a reduced permeability caused an increase of the apparent intra-axonal water volume. Concerning the differences in myelin T_2, in this work we observed that parameters estimation was much more different across n_{wraps} in long T_2 than in short although some interesting slight differences could be observed for lower number of wraps in clinical acquisition setting.

The Kärger model fit well to all the simulated signals. Estimates of exchange times were aligned with expectations in those cases where τ was on the sub-second scale, e.g. for small axons and up to approximately 8 wraps. For longer ground-truth exchange times, the estimated exchange times were associated to large errors. This was due to the negligible effect of exchange on the signal for those longer exchange times. Concerning v_{ic}, the estimated values had negligible error, with values in a range comprehending the ground truth. Also ADC_{ec} findings were stable, showing a very slight dependence from d_{inner} while it resulted independent from n_{wraps}. The resulting values were in agreement with D/λ (λ corresponding to tortuosity factor) as in [7]. An important implication derived by our work is added evidence of the capability of Kärger model to retrieve τ when n_{wraps} is low such as in the developing brain or in case of demyelinating diseases [32], [33]. Furthermore, in these cases relaxometry modeling may be unnecessary because the impact of compartmental differences in T_2 relaxation times was minimal.

TABLE I
OBSERVABLE AND FITTED EXCHANGE TIME WITH 5^{th} AND 95^{th} PERCENTILES REPORTED FOR EACH AXON DIAMETER AND NUMBER OF WRAPS IN ANALYSIS

d_{inner} [μm]	n_{wraps}	Obs τ [ms]	Fit τ ($5^{th} - 95^{th}$) [ms]
1.0	1	126	120 (112 – 130)
	2	251	237 (223 – 255)
	4	507	543 (495 – 596)
	8	1077	770 (688 – 863)
	16	2761	2381 (1883 – 3351)
	32	5254	2608 (2057 – 3458)
2.0	1	1015	780 (702 – 882)
	2	2026	1301 (1105 – 1569)
	4	4104	2059 (1652 – 2664)
	8	9005	3215 (2270 – 5103)
	16	16718	2473 (1937 – 3475)
	32	19805	2681 (2047 – 3717)

The simulation substrate that was used in the present study oversimplifies the white matter microstructures, which leads to some limitations. First, we assumed a square axonal packing. This allows a maximum v_{ic} lower than what would correspond to a hexagonal one [37]. It also prevents the appearance of time-dependent diffusion in the extracellular space, which results from random packing [38], [39]. Second, white matter contains axons with a distribution of diameters [40]. This limits the exploitability of the proposed model for the interpretation of *in-vivo* measurements. Third, exchange through the successive bilayers that make up the myelin spiral should also be accounted for. For thick axons with multiple wraps, we expect this exchange mechanism to dominate over the spiral mechanism investigated here. Fourth, the simulations of the diffusion in the myelin wraps were performed using another stepping mechanism than in the intra- and extra-axonal spaces and this could have an impact on the effective diffusivity in the spiral. In future work, simulations based on digitized high-resolution models of brain cells will be considered [41]. Despite these limitations, our results show that in thin axons with few wraps, exchange through the myelin spiral should not be neglected in dMRI modeling since this mechanism alone can contribute to sub-second exchange times.

V. CONCLUSION

The present study explores the impact of the spiraling myelin structure on the rate of water exchange between intra- and extra-axonal environments, and its influence on the dMRI signal. Our analysis predicts sub-second exchange times for small axons ($d_{\text{inner}} < 2.0$ μm) and low number of myelin turns ($n_{\text{wraps}} < 16$). Our results thus suggest that geometric models must take diffusion through the spirals into account for thin axons with few wraps. Axons in healthy white matter can be expected to have more than 8 wraps and unless some other exchange mechanism contributes substantially to the exchange, we can expect slow exchange. On the other hand, axons with fewer wraps are found in the infant brain and in demyelinating diseases, which may result in sub-second and clinically detectable exchange times.

REFERENCES

[1] S. N. Sotiropoulos and A. Zalesky, "Building connectomes using diffusion MRI: Why, how and but," *NMR Biomed.*, Jun. 2017, Art. no. e3752. doi: 10.1002/nbm.3752.

[2] Y. Assaf, T. Blumenfeld-Katzir, Y. Yovel, and P. J. Basser, "Axcaliber: A method for measuring axon diameter distribution from diffusion MRI," *Magn. Reson. Med.*, vol. 59, no. 6, pp. 1347–1354, 2008.

[3] S. Lasič, F. Szczepankiewicz, S. Eriksson, M. Nilsson, and D. Topgaard, "Microanisotropy imaging: Quantification of microscopic diffusion anisotropy and orientational order parameter by diffusion MRI with magic-angle spinning of the q-vector," *Frontiers Phys.*, vol. 2, p. 11, Feb. 2014.

[4] F. Szczepankiewicz *et al.*, "Quantification of microscopic diffusion anisotropy disentangles effects of orientation dispersion from microstructure: Applications in healthy volunteers and in brain tumors," *NeuroImage*, vol. 104, pp. 241–252, Jan. 2015.

[5] C.-F. Westin *et al.*, "Q-space trajectory imaging for multidimensional diffusion MRI of the human brain," *NeuroImage*, vol. 135, pp. 345–362, Jul. 2016.

[6] M. Nilsson, J. Lätt, E. Nordh, R. Wirestam, F. Ståhlberg, and S. Brockstedt, "On the effects of a varied diffusion time *in vivo*: Is the diffusion in white matter restricted?" *Magn. Reson. Imag.*, vol. 27, no. 2, pp. 176–187, 2009.

[7] M. Nilsson, E. Alerstam, R. Wirestam, F. Ståhlberg, S. Brockstedt, and J. Lätt, "Evaluating the accuracy and precision of a two-compartment Kärger model using Monte Carlo simulations," *J. Magn. Reson.*, vol. 206, no. 1, pp. 59–67, 2010.

[8] M. Nilsson, H. Hagslätt, D. Van Westen, R. Wirestam, F. Ståhlberg, and J. Lätt, "A mechanism for exchange between intraaxonal and extracellular water: Permeable nodes of Ranvier," in *Proc. Int. Soc. Magn. Reson. Med.*, Stockholm, Sweden, vol. 18, 2010, p. 1570.

[9] M. Nilsson *et al.*, "Noninvasive mapping of water diffusional exchange in the human brain using filter-exchange imaging," *Magn. Reson. Med.*, vol. 69, no. 6, pp. 1572–1580, 2013.

[10] M. Nilsson, D. van Westen, F. Ståhlberg, P. C. Sundgren, and J. Lätt, "The role of tissue microstructure and water exchange in biophysical modelling of diffusion in white matter," *Magn. Reson. Mater. Phys., Biol. Med.*, vol. 26, no. 4, pp. 345–370, 2013.

[11] J. M. Edgar and I. R. Griffiths, "White matter structure: A microscopist's view," in *Diffusion MRI*, H. Johansen-Berg and T. E. Behrens, Eds. San Diego, CA, USA: Academic, 2009, pp. 74–103.

[12] T. Paus, "Growth of white matter in the adolescent brain: Myelin or axon?" *Brain Cognition*, vol. 72, no. 1, pp. 26–35, 2010.

[13] K. P. Whittall, A. L. Mackay, D. A. Graeb, R. A. Nugent, D. K. B. Li, and D. W. Paty, "*In vivo* measurement of T_2 distributions and water contents in normal human brain," *Magn. Reson. Med.*, vol. 37, no. 1, pp. 34–43, 1997.

[14] G. L. Nedjati-Gilani *et al.*, "Machine learning based compartment models with permeability for white matter microstructure imaging," *NeuroImage*, vol. 150, pp. 119–135, Apr. 2017.

[15] E. Fieremans, D. S. Novikov, J. H. Jensen, and J. A. Helpern, "Monte Carlo study of a two-compartment exchange model of diffusion," *NMR Biomed.*, vol. 23, no. 7, pp. 711–724, 2010.

[16] S. N. Hwang, C.-L. Chin, F. W. Wehrli, and D. B. Hackney, "An image-based finite difference model for simulating restricted diffusion," *Magn. Reson. Med.*, vol. 50, no. 2, pp. 373–382, 2003.

[17] P. N. Sen and P. J. Basser, "A model for diffusion in white matter in the brain," *Biophys. J.*, vol. 89, no. 5, pp. 2927–2938, 2005.

[18] S. Peled, "New perspectives on the sources of white matter DTI signal," *IEEE Trans. Med. Imag.*, vol. 26, no. 11, pp. 1448–1455, Nov. 2007.

[19] G. T. Baxter and L. R. Frank, "A computational model for diffusion weighted imaging of myelinated white matter," *NeuroImage*, vol. 75, pp. 204–212, Jul. 2013.

[20] K. D. Harkins and M. D. Does, "Simulations on the influence of myelin water in diffusion-weighted imaging," *Phys. Med. Biol.*, vol. 61, no. 13, p. 4729, 2016.

[21] J. H. Jensen, J. A. Helpern, A. Ramani, H. Lu, and K. Kaczynski, "Diffusional kurtosis imaging: The quantification of non-Gaussian water diffusion by means of magnetic resonance imaging," *Magn. Reson. Med.*, vol. 53, no. 6, pp. 1432–1440, 2005.

[22] J. Kärger, H. Pfeifer, and W. Heink, "Principles and application of self-diffusion measurements by nuclear magnetic resonance," in *Advances in Magnetic and Optical Resonance*, vol. 12, J. S. Waugh, Ed. New York, NY, USA: Academic, 1988, pp. 1–89.

[23] D. Liewald, R. Miller, N. Logothetis, H.-J. Wagner, and A. Schüz, "Distribution of axon diameters in cortical white matter: An electron-microscopic study on three human brains and a macaque," *Biol. Cybern.*, vol. 108, no. 5, pp. 541–557, 2014.

[24] G. M. Innocenti, R. Caminiti, and P. R. Hof, "Fiber composition in the *planum temporale* sector of the *corpus callosum in chimpanzee* and human," *Brain Struct. Function*, vol. 215, no. 2, pp. 123–128, 2010.

[25] D. Raffelt *et al.*, "Apparent fibre density: A novel measure for the analysis of diffusion-weighted magnetic resonance images," *NeuroImage*, vol. 59, no. 4, pp. 3976–3994, 2012.

[26] M. Nilsson, S. Lasič, I. Drobnjak, D. Topgaard, and C.-F. Westin, "Resolution limit of cylinder diameter estimation by diffusion MRI: The impact of gradient waveform and orientation dispersion," *NMR Biomed.*, vol. 30, no. 7, p. e3711, 2017.

[27] J. Pfeuffer, U. Flögel, W. Dreher, and D. Leibfritz, "Restricted diffusion and exchange of intracellular water: Theoretical modelling and diffusion time dependence of ^{1}H NMR measurements on perfused glial cells," *NMR Biomed.*, vol. 11, no. 1, pp. 19–31, 1998.

[28] J. D. Quirk *et al.*, "Equilibrium water exchange between the intra- and extracellular spaces of mammalian brain," *Magn. Reson. Med.*, vol. 50, no. 3, pp. 493–499, 2003.

[29] R. D. Dortch, K. D. Harkins, M. R. Juttukonda, J. C. Gore, and M. D. Does, "Characterizing inter-compartmental water exchange in myelinated tissue using relaxation exchange spectroscopy," *Magn. Reson. Med.*, vol. 70, no. 5, pp. 1450–1459, 2013.

[30] A. N. Dula, D. F. Gochberg, H. L. Valentine, W. M. Valentine, and M. D. Does, "Multiexponential T_2, magnetization transfer, and quantitative histology in white matter tracts of rat spinal cord," *Magn. Reson. Med.*, vol. 63, no. 4, pp. 902–909, 2010.

[31] K. D. Harkins, A. N. Dula, and M. D. Does, "Effect of intercompartmental water exchange on the apparent myelin water fraction in multiexponential T_2 measurements of rat spinal cord," *Magn. Reson. Med.*, vol. 67, no. 3, pp. 793–800, 2012.

[32] K.-J. Chang, S. A. Redmond, and J. R. Chan, "Remodeling myelination: Implications for mechanisms of neural plasticity," *Nature Neurosci.*, vol. 19, no. 2, pp. 190–197, 2016.

[33] M. Albert, J. Antel, W. Brück, and C. Stadelmann, "Extensive cortical remyelination in patients with chronic multiple sclerosis," *Brain Pathol.*, vol. 17, no. 2, pp. 129–138, 2007.

[34] F. Barkhof and M. van Walderveen, "Characterization of tissue damage in multiple sclerosis by nuclear magnetic resonance," *Philos. Trans. Roy. Soc. London B, Biol. Sci.*, vol. 354, no. 1390, pp. 1675–1686, 1999.

[35] L. Ning, M. Nilsson, S. Lasič, C.-F. Westin, and Y. Rathi, "Cumulant expansions for measuring water exchange using diffusion MRI," *J. Chem. Phys.*, vol. 148, no. 7, 2018, Art. no. 074109.

[36] G. J. Stanisz, G. A. Wright, R. M. Henkelman, and A. Szafer, "An analytical model of restricted diffusion in bovine optic nerve," *Magn. Reson. Med.*, vol. 37, no. 1, pp. 103–111, 1997.

[37] M. G. Hall and D. C. Alexander, "Convergence and parameter choice for Monte-Carlo simulations of diffusion MRI," *IEEE Trans. Med. Imag.*, vol. 28, no. 9, pp. 1354–1364, Sep. 2009.

[38] L. M. Burcaw, E. Fieremans, and D. S. Novikov, "Mesoscopic structure of neuronal tracts from time-dependent diffusion," *NeuroImage*, vol. 114, pp. 18–37, Jul. 2015.

[39] N. Sapkota *et al.*, "Characterization of spinal cord white matter by suppressing signal from hindered space. A Monte Carlo simulation and an *ex vivo* ultrahigh-b diffusion-weighted imaging study," *J. Magn. Reson.*, vol. 272, pp. 53–59, Nov. 2016.

[40] F. Aboitiz, A. B. Scheibel, R. S. Fisher, and E. Zaidel, "Fiber composition of the human corpus callosum," *Brain Res.*, vol. 598, nos. 1–2, pp. 143–153, 1992.

[41] M. Palombo, D. C. Alexander, and H. Zhang, "A generative model of realistic brain cells with application to numerical simulation of the diffusion-weighted MR signal," *NeuroImage*, vol. 188, pp. 391–402, Mar. 2019.